Domain-Growth Kinetic Origin of Nonhorizontal Phase Coexistence Plateaux in Langmuir Monolayers: Compression Rigidity of a Raft-Like Lipid Distribution

ARTICLE *in* THE JOURNAL OF PHYSICAL CHEMISTRY B · MARCH 2010

Impact Factor: 3.3 · DOI: 10.1021/jp9118953 · Source: PubMed

4 AUTHORS:

Laura Arriaga
Harvard University
30 PUBLICATIONS **354** CITATIONS
SEE PROFILE

Ivan Lopez-Montero
Complutense University of Madrid
36 PUBLICATIONS **606** CITATIONS
SEE PROFILE

Jordi Ignes-Mullol
University of Barcelona
71 PUBLICATIONS **552** CITATIONS
SEE PROFILE

Francisco Monroy
Complutense University of Madrid
103 PUBLICATIONS **1,590** CITATIONS
SEE PROFILE

Domain-Growth Kinetic Origin of Nonhorizontal Phase Coexistence Plateaux in Langmuir Monolayers: Compression Rigidity of a Raft-Like Lipid Distribution

Laura R. Arriaga,[†] Iván López-Montero,[†] Jordi Ignés-Mullol,*[,‡] and Francisco Monroy*[,†]

Mechanics of Biological Membranes and Biorheology, Departamento de Química Física I, Universidad Complutense de Madrid, 28040 Madrid, Spain, and Departamento de Química Física, Universidad de Barcelona, Martí i Franquès 1, 08028 Barcelona, Spain

Received: December 16, 2009; Revised Manuscript Received: February 15, 2010

The present work addresses the question of a nonhorizontal coexistence plateau found in the liquid-expanded (LE) to liquid-condensed (LC) transition of Langmuir monolayers of lipid amphiphiles, which is apparently incongruent with the first-order character of this main LE/LC phase transition. This pathology is understood in a mechanical context as a resistance of the monolayer against compression giving rise to a nonzero rigidity in the coexistence region. Surface rheology has allowed for a quantitative determination of the compression parameters, namely, dilational elasticity ε and viscosity η. Data for the phase coexistence region reveal dynamical stiffening at faster deformation, which points out a chief control of lipid diffusion on monolayer rigidity. Monolayer viscosity remains however low at the value corresponding to the continuous fluid phase. The presence of coexistence domains is then invoked as the structural element responsible for such a nontrivial rheology, the finite domain growth rate imposing a kinetic limit for equilibrium compression along a quasi-static path. Brewster angle microscopy has allowed for studying the kinetic mechanism for domain growth. The finite rigidity observed at the coexistence region is related to the resistance of LC domains to grow at the expense of the LE phase. A reconciliation of the nonhorizontal plateau observed at finite compression rates with the first-order character of the LE/LC transition emerges then naturally from this kinetic scenario. New mechanical features are consequently assigned to the phase-separated monolayers made of stiff grains rafting in a fluid matrix. Particularly, for a raft-like lipid distribution, we hypothesize a finite rigidity kinetically controlled by the rate of domain growth and a high fluidity controlled by the continuous phase. We have depicted a minimal model of membrane mechanics that accounts for the elasticity of such a heterogeneous composite medium. This "Plum-cake" model is able to qualitatively predict the observed mechanical features and is suggested to describe raft-like membranes as compliant elastic media where lipid domains work as reservoirs able to exchange material with the surrounding fluid phase.

Introduction

Langmuir monolayers of fatty amphiphiles are known to undergo different structural transitions easily identifiable in the surface pressure isotherm measured at varying surface area (see classical reviews in refs 1–4). This method is primarily thermodynamic; therefore, it provides no direct information about the microscopic nature of the monolayer but only on the character of the surface phases and the transitions between them. Early workers recognized the existence of a complex monolayer polymorphism depending on the chemical structure and thermodynamic variables mainly defined by lateral packing and temperature.[5,6] Specific surface microscopy techniques, fluorescence and Brewster angle methods for instance, have enabled a detailed description of the monolayer textures corresponding to the different monolayer phases appearing as a consequence of lateral packing. Molecular packing is usually varied as the surface area available to the monolayer is decreased under continuous lateral compression exerted by the barriers of the Langmuir trough. However, kinetic effects related to relatively high compression speeds give rise to metastable states which have been frequently invoked as a plausible source for unexpected monolayer features, such as the subtle structural differences between hypothetic different solid phases at high packing[6] or the nonhorizontal nature of the coexistence plateaux exhibited by a variety of lipid monolayers.[7]

As far as a lipid bilayer consists of two weakly coupled monolayers, monolayers of phospholipids have been traditionally studied as models of biological membranes.[1,3,8] In analogy with the structural fluid-to-gel transition of bilayer membranes, the main transition of phospholipid monolayers is observed at a given pressure defining the coexistence plateau between the liquid-condensed disperse phase (LC ≡ gel) growing at the expense of the continuous liquid-expanded phase (LE ≡ fluid). The nature of this main LE/LC phase transition has been much discussed, being most frequently suggested to be of first order as an isothermal coexistence between two phases is observed in microscopy experiments.[1–4,8–10] However, nonhorizontal isotherm slopes are usually found in continuous compression experiments performed at a standard finite rate; thereby, the LE/LC transition has been frequently claimed to be higher order.[1,9] On the finding that isotherm slopes are reduced under electrostatic screening, alternative explanations have included long-range repulsive forces between polar heads as a possible source of plateau nonhorizontality.[11,12] However, any realistic estimate of electrostatic effects, even for charged phospholipids, yields a too low contribution to surface tension to ascribe the observed slopes to these forces.[1]

* To whom correspondence should be addressed.
[†] Universidad Complutense de Madrid.
[‡] Universidad de Barcelona.

10.1021/jp9118953
Published on Web 03/17/2010

Pallas and Pethica were who first hypothesize impurities as the source of this thermodynamic pathology observed in monolayers of fatty acids.[13,14] Those authors revealed a near-horizontal slope when highly purified pentadecanoic acid is used in obtaining monolayer states by dropwise addition.[13,14] They were able, for the first time, to give experimental evidence of the first-order character of the LE/G and LE/LC transitions, although they also recognized the fact that under lateral compression, markedly nonzero slopes are systematically obtained, even for the highest-purity samples. Later, upon the recognition that impurities have strong effects on monolayer thermodynamics, Hifeda and Rayfield performed a systematic study of the requirements for a zero slope in the LE/LC coexistence region; these include pure materials, ultraclean experimental conditions, accurate temperature and humidity control, and extremely slow compression rates.[15] On the idea that the nonhorizontal behavior is exclusively due to impurities, the Monte Carlo simulations performed by Georgallas and Pink pointed out that at least 4% impurities are necessary to produce theoretical $\pi-A$ isotherms with a significant slope in the transition region.[16] Roland et al. developed a model which indicated that nonequilibrium behavior also contributes to a nonzero slope in the LE/LC transition region, particularly at rapid continuous compression.[17] In that model, the LE/LC is a well-defined first-order transition where finite-size coexistence domains are metastable structures formed when the monolayer is compressed. Domain metastability is introduced in a way such that domain size is linked with the conformational state of the lipid chains via the accessible free volume, which remains higher at faster compression.[17] The conclusion is that at ideal equilibrium, complete first-order phase separation is accomplished with a minimum free volume inside of the LC phase, but fast compression induces a partial segregation into finite-sized metastable domains, resulting in a "nonequilibrium" phase coexistence state characterized by a nonhorizontal plateau.

As the debate remains still open, we propose an integrative hypothesis grounded on the macroscopic connection between the mechanical rigidity of a microheterogeneous medium made of two coexisting phases and frustrated first-order metastable energetics giving rise to a nonhorizontal transition plateau. The present work focuses indeed on the possible influence of lipid domains on the in-plane compression mechanics of model membranes. In this work, we capture the idea of finite membrane rigidity due to the presence of domains with a given resistance to grow under lateral compression in the coexistence region. Consequently, the nonzero values of the dilational modulus usually observed in this region will be attributed to a transitory resistance effect due to a dynamically limited transport between the continuous phase and the domains. Only at ideal kinetically nonlimited equilibrium conditions, similar to those existing in the discontinuous dropwise experiments[13,14] or quasi-static ones performed at an extremely low compression rate,[15] will the phase transition be found strictly first-order and the compression modulus null. A meaningful study of this domain influence requires an ability of monitoring rate-dependent compression viscoelasticity in a broad range of domain sizes and concentrations. Supported by experimental evidence, we will depict a minimal model of surface viscoelasticity for such a raft-like lipid distribution. The model, which we call the Plum-cake picture, considers lipid domains as a mechanical active element of structure able to exchange lipids with the continuous phase. These mechanical ideas can be eventually connected with the increasingly accepted picture of biological membranes as heterogeneous bilayer structures.[18–22] As a main consequence of our results, we will suggest raft domains as an active structural element able to confer special elasticity features to biological membranes.

Materials and Methods

Model Monolayer. The above problem is addressed by studying the dilational rheology of Langmuir monolayers of a model phospholipid at the phase-separated state. Particularly, dipalmitoylphosphocholine (DPPC) is a fully saturated zwitterionic phospholipid able to pack at different bilayer states corresponding to homogeneous monolayer phases. The relevant monolayer phases are (a) liquid-expanded (LE), which is a low-density fluid where the acyl chains are at a disordered state, (b) liquid-condensed (LC), which is formed upon lateral compression with the tilted acyl chains ordered parallel, and (c) solid (S), where the ordered chains become perpendicular to the monolayer plane in a hexagonal crystalline arrangement. LE is the structural analogue of the bilayer fluid state characteristic of the fluid matrix of biological membranes, and LC is of the gel state typical of lipid rafts enriched in saturated chains. Specifically, although lipid rafts are not based in saturated phospholipids, DPPC is found as a main component of plasma and organelle membranes[23–26] and represent a large fraction in pulmonary surfactant films.[27–30]

Chemicals. 1,2-Dipalmitoyl-*sn*-glycero-3-phosphocholine (DPPC) was purchased from Avanti Polar Lipids (Alabaster, AL) at 99% purity and used as received. In source, it is purified by HPLC to the highest purity commercially available; therefore, spurious effects due to impurities might be reasonably discarded. Special precautions are taken to protect the product for oxidization and hydrolysis (the solid powder is stored at −80 °C, and the chloroform spreading solutions are freshly prepared). HPLC-grade chloroform filtered through 0.2 μm membranes (Chromasolv) was from Sigma. Deionized water for the aqueous subphase was obtained from a Milli-Q unit with a filtration system which produces highly deionzed water (resistivity higher than 18 Mohm cm) with a very small organic matter content (<2 ppb). The water surface tension is routinely checked to be $\gamma_0 = 72.2 \pm 0.1$ mN/m at 25 °C.

Surface Pressure Isotherms. To spread DPPC as Langmuir monolayers, we use ∼1 mg/mL solutions of the lipid in chloroform. A 100 μL Hamilton syringe was used to drop these lipid solutions on an aqueous subphase contained in a Langmuir trough NIMA 702BAM (Nima Technology, U.K.). The surface area of the Teflon trough was $A_0 = 720$ cm^2 (72 cm long, 10 cm wide, and 5 mm deep). The whole setup was enclosed inside a Plexiglas box with small windows for inserting the dispensing syringe. The surface laboratory room was air-conditioned at 22 °C and slightly overpressurized to avoid dust suspension. The temperature was controlled in the subphase by a thermostatic bath pumping water to a jacket in the trough bottom and in the atmosphere by two black-light IR lamps driven by a contact thermometer. For this device, the temperature control in the subphase was better than ±0.1 at 25 °C. The humidity was controlled at experimental temperature by saturating the inner box atmosphere with a water-swollen filter paper. The surface tension was measured by a paper Wilhelmy plate (Whatman CHR1 chromatography paper, effective perimeter 21 mm, supplied by NIMA), ensuring a zero-angle contact angle. Before an acceptable monolayer experiment, the bare surface of the water subphase was repeatedly swept by compression and surface aspiration using a Teflon pipe connected to a vacuum line. The process was repeated as many times as necessary until constant surface tension ($\gamma_0 = 72.2$ mN/m, under barrier

compression). Surface pressure−area isotherms and oscillatory barrier measurements were recorded as the monolayer was uniaxially compressed under the action of the barriers of the trough. Each experiment was begun with a freshly cleaned apparatus following a strict cleaning protocol based on a strong nonionic detergent (Decon) and alternate washing out with high-purity solvents (gently hot water, acetone, and chloroform).

Brewster Angle Microscopy. The Langmuir trough was adapted to a homemade Brewster angle microscope (BAM). Briefly, a custom-made double optomechanical arm enables one to send spatially filtered and collimated laser light from a diode module (MC6535, Monocrom S.L., Spain; 25mW, $\lambda = 650$ nm) onto the air/water interface at the Brewster angle. The incident beam is linearly polarized in the plane of incidence by a Glann−Thomson polarizer. The reflected beam is collected by a Nikon 4× objective mounted on the second arm. It is modulated by a Glann−Thomson polarizer and directed onto a CCD camera (JAI), which records the BAM image of the observed region (2×2 mm^2). Further image processing is performed by the public domain software ImageJ.[31] This setup is compared with a commercial microscope EP^3-BAM (Nanofilm Tech., DE), obtaining similar images of domain textures. The visualization of lipid microdomains along phase coexistence regions is performed by Brewster angle microscopy.[32,33] Spatial reflectivity modulations are correlated to coexistence of optically different monolayer phases with different packing density or lateral ordering. Phases with long-range orientational order result in modulations in the polarization state of the reflected light, which result in characteristic bright textures in BAM images, which may be analyzed to understand the molecular arrangement and to measure material parameters from the system.[34]

Statistical Population Analysis. Domain size distribution has revealed the presence of three different populations at each surface pressure state. The number of domains N in each population has been fitted to a normal Gaussian distribution as given by

$$N(A) = \frac{a}{\sqrt{2\pi w A}} \exp\left[-\frac{\ln(A/A_c)}{2w^2}\right] \quad (1)$$

This distribution reaches it maximum value for a molecular area value A_{max}, which is a value smaller than the one that corresponds to the center of the distribution A_c, $A_{max} = A_c \exp(-w^2)$. The characteristic size of the smallest population observed at each surface pressure state is practically at the resolution limit of the microscope; thus, it has been attributed to pixelization noise. The other two populations can be assigned to domain sizes as they appear just after starting nucleation and disappear beyond the phase coexistence boundaries.

Oscillatory Barrier Rheology. This method has been thoughtfully described elsewhere.[35,36] Both the amplitude u_0 and period ($= 2\pi/\omega$) of the applied surface dilation are controlled by the sinusoidal motion of the barriers of the Langmuir trough, which impose the available area to change in a fashion

$$A(t) = A_0\left[1 + \frac{u_0}{2}\sin(\omega t + \phi_u)\right] \quad (2)$$

where A_0 is the initial area, $u_0 = (A - A_0)/A_0$ is the relative deformation amplitude, ω is the frequency of the oscillatory motion, and ϕ_u accounts for a possible initial phase.

The stress response is measured by the pressure sensor and monitored as a function of time, taking a reading every 1 s. At small deformations, $u_0 \to 0$, the stress response $\sigma(t)$ dependence closely follows a sinusoidal profile of frequency ω equal to that of the strain wave

$$\sigma(t) = \Pi(t) - \Pi_0 = \frac{\sigma_0}{2}\sin(\omega t + \phi_\pi) \quad (3)$$

where Π_0 is the initial pressure, σ_0 the stress amplitude, and ϕ_π a phase factor accounting for the delay imposed by viscous friction within the response. This is characteristic of a viscoelastic linear regime; thus, the frequency-dependent linear dilational viscoelastic modulus is a strain-independent parameter which can be calculated from the causality relationship in eq 4 Here, the dilational stress $\sigma(t)$ acts as a longitudinal restoring

$$\sigma(t) = (\varepsilon + i\omega\eta)\cdot u(t) \quad (4)$$

force for recovering the initial state of the monolayer when strain is at the dilating semicycle. Indeed, eq 4 is formally equivalent to a combination of Hooke's law for an elastic body and Newton's law for linear viscous flow. The proportionality factors are respectively the elastic modulus ε and the dilational viscosity η, both including compression plus shear components. For small-amplitude oscillatory motion, $u(t) \approx u_0 e^{i\omega t}$, with frequency ω, the presence of the viscous term imposes some delay ϕ in the viscoelastic response, $\sigma(t) = \sigma_0 e^{i(\omega t+\phi)}$, which is measurable as the phase difference between stress and strain, that is, $\phi = \phi_\pi - \phi_u$. The modulus of the complex viscoelasticity in eq 4 determines the amplitude of the stress response

$$\frac{\sigma_0}{u_0} = (\varepsilon^2 + \omega^2\eta^2)^{1/2} \quad (5)$$

and the phase difference ϕ is determined by the losses-to-storage ratio

$$tg\phi = \frac{\omega\eta}{\varepsilon} \quad (6)$$

In a typical oscillatory barrier experiment, the dilational parameters are calculated from experimentally averaged parameters (σ_0/u_0 and ϕ) obtained by comparison between the strain−stress time traces. The dilational elasticity modulus ε and the dilational viscosity η are then calculated as

$$\begin{aligned} \varepsilon &= (\sigma_0/u_0)\cos\phi \\ \eta &= (\sigma_0/\omega u_0)\sin\phi \end{aligned} \quad (7)$$

Results and Discussion

Surface Pressure Isotherm. The Langmuir monolayers of the model phospholipid DPPC have been extensively studied.[8,37,38] Figure 1a plots the room -temperature surface pressure isotherm (Π−A at $T = 25.0 \pm 0.1$ °C) obtained upon continuous unilateral compression at the slowest rate instrumentally accessible ($-dA/dt = 10$ cm^2/min; $R_{comp} = -(2/A_0)(dA/dt) = 1.15 \times 10^{-4}$ s^{-1}). These data are similar to previous ones reported in the literature at similar conditions.[8,37,38] At room temperature, the system transits from a gaseous phase at extremely low

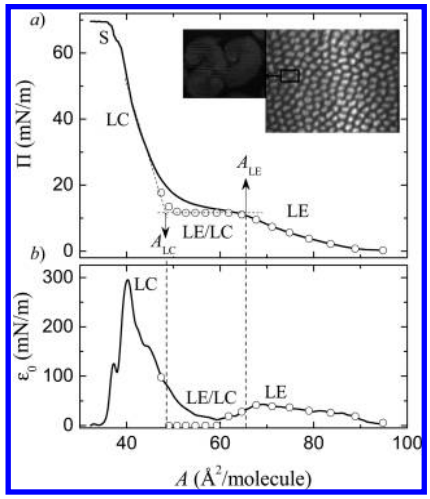

Figure 1. (a) Surface pressure−area isotherm of the DPPC Langmuir monolayer at 25 °C. The curve has been obtained by compressing the monolayer at a constant barrier speed of 10 cm²/min. The different monolayer phases are denoted as follows: LE: liquid-expanded; LC: liquid-condensed (the LC boundary A_{LC} is obtained as the intercept between the extrapolated plateau and the LC phase; dashed lines); LE/LC: phase coexistence region. The symbols correspond to single shot data obtained at equilibrium conditions after dropwise addition. Inset: Images showing BAM textures at coexistence for the monolayer at 25 °C. (b) Compression modulus values of DPPC Langmuir monolayers at 25 °C (from the numerical derivative of the Π−*A* isotherm in Figure 1a, calculated over 100 interpolated points to avoid spurious finite difference noise). The symbols correspond to the equilibrium compression modulus as calculated from the single shot data in (a).

pressure ($\Pi \approx 0$) to a LE phase. This LE phase retains the fluid character imposed by the disordered in-plane organization of the polar heads, but at surface density high enough, the acyl chains can eventually organize nematic-like. This phase is structurally homologue to the liquid crystalline phase (L_α) characteristic of the lyotropic bulk state.[39,40] At a given packing molecular area, $A_{LE} \approx 64$ Å², the system enters a phase coexistence region and transits from the LE fluid state to a highly ordered condensed state characterized by a much lower fluidity.[40] This onset is found at a similar molecular area as that in the quasi-static isotherm measured for DPPC with a similar purity by Hifeda and Rayfield.[15] At the phase boundary A_{LE}, the LC phase starts to nucleate as bean-shaped three-arm domains.[1–4,37,40] The *sn*-DPPC enantiomer is known to form left-handed chiral structures (see inset in Figure 1). The presence of internal order endows domains with an anisotropic distribution of the line tension.[1–4] This feature is relevant as it imposes the domains to grow along a preferential direction.[3,41–44] The LC phase grows throughout the coexistence plateau as further domain growth and nucleation develop under lateral compression. It involves a discontinuous change in density at constant surface pressure; the LE/LC phase transition might occur at constant pressure, that is, it should be ideally first-order, $(\partial\Pi/\partial A)_T \approx 0$, as observed by Hifeda and Rayfield in compressing laterally at a very low rate ($R_{comp} \approx 3 \times 10^{-5}$ s^{-1}).[15] However, in our compression experiment, performed at the minimal rate accessible to the NIMA instrument ($R_{comp} \approx 10^{-4}$ s^{-1}),[45] the LE−LC plateau region is found to be nonhorizontal, similar to previous data performed at standard conditions.[1,8,9,37,38] The LC phase boundary A_{LC} appears as a smooth increasing branch in the Π−*A* isotherm, its precise identification becoming challenging as it requires a macroscopic verification of homogeneous LC phase re-entrance. We identify A_{LC} as the crossover point between adjacent linear behavior (see the details in Figure 1).

Further insight is gained from the dropwise isotherm obtained as discrete states reached by consecutive single shots of the lipid chloroform solution. In this method, each pressure point is measured after waiting 30 min for monolayer equilibration. As shown by Figure 1, single shot data perfectly superpose the compression isotherm at the homogeneous LE state. Furthermore, a near-horizontal plateau is found at the LE/LC coexistence region, the A_{LE} boundary appearing at identical molecular area as that in the continuous isotherm ($A_{LE} \approx 64$ Å²). The onset of the LC single-phase re-entrance also nearly coincides with the value estimated from the compression isotherm ($A_{LC} \approx 48$ Å²). In effect, the data confirm (1) the first-order character of the equilibrium LE/LC transition, (2) an acceptably high degree of chemical purity, and (3) the metastable character of the surface states reached by continuous compression at a finite rate.

Dilational Modulus. The dilational modulus measures the elastic energy stored by the monolayer upon the unilateral compression stressed by the barriers of the Langmuir trough

$$\varepsilon_0 = -A\left(\frac{\partial \Pi}{\partial A}\right)_T \tag{8}$$

This elasticity parameter characterizes the rigidity of the monolayer upon quasi-static uniaxial dilation, which actually contains hydrostatic compression plus shear components, $\varepsilon = K + G$.[46] Disordered fluid monolayers are characterized by a small dilational modulus (high compressibility, $K \leq 50$ mN/m; absolute shear compliance, $G \equiv 0$), while high values ($\varepsilon > 50$ mN/m) are typical of structurally rigid monolayers for which small deformations are followed by large changes in surface pressure.

Figure 1b shows the dilational modulus for DPPC monolayers obtained from the numerical derivative of the Π−*A* isotherms in Figure 1a. Two different maxima corresponding to LE and LC phases are clearly identified. The maximum at large area corresponds to the high compressibility LE state ($\varepsilon_0 \leq 50$ mN/m). The LC phase is characterized by comparatively higher values of the dilational elasticity (at the maxima, $\varepsilon_0 \approx 300$ mN/m), as expected for a condensed ordered phase. Similarly to the homologue gel phase of the lamellar state, orientational degrees of freedom are frozen in the LC phase of DPPC monolayers, allowing them to support shear elasticity. However, this soft gel-like LC phase is characterized by low values of shear modulus ($G \approx 1$ μN/m)[47,48] as compared to the compression component modulus ($K \approx 300$ mN/m), which essentially determines the dilational response ($\varepsilon = K + G \approx K$).[49]

At the coexistence plateau, which is the strong thermodynamic consequence of nucleation of the LC phase at the expense of the LE (ideally first-order), we observe, however, finite compression rigidity, $\varepsilon_0 > 0$. Similarly to previous literature data,[1–4,37] the coexistence plateau is found to be nonhorizontal but weakly increasing upon lateral compression (see Figure 1); thus, finite values of the dilational modulus are measured in this region (see data in Figure 1b), in contrast with the expected thermodynamic value which might ideally be 0, that is, $\varepsilon_0^{(coex)} = -A(\partial\Pi/\partial A)_{ideal} = 0$, and calculated from the true equilibrium (dropwise) isotherm (see Figure 1b). As said in the Introduction, earlier explanations pointed to surface impurities as a plausible reason for the successive nucleation of different species, depending on the compression conditions;[37] however, this possibility can be reasonably ruled out as similar results are obtained with high-purity and doped lipids.[1,50] It is worthy noticing that the possible concomitance of shear effects arising from the gel-like LC phase might be limited to a negligibly

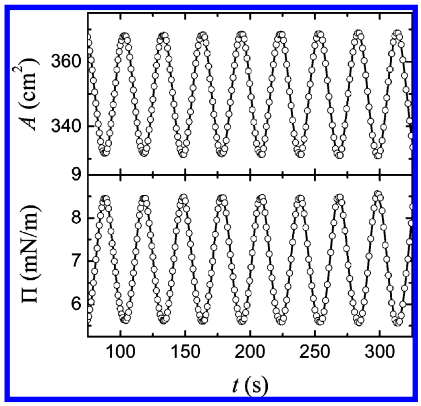

Figure 2. Stress/strain variation with time in the linear regime. The open circles represent the experimental data, and the lines represent the fitting functions for (a) area variation fitted by using $A(t) = A_0 + (\Delta A/2)\cos(\omega t + \phi_u)$ and (b) surface pressure variation in response to the applied deformation fitted by using $\Pi(t) = \Pi_0 + (\Delta\Pi/2)\cos(\omega t + \phi_\pi)$.

small component ($G \approx 1$ μN/m) on the whole dilational response ($\varepsilon = K + G$). In other words, possible shear components arising from the solid-like character of LC domains might contribute residually to the observed compression rigidity at the coexistence region. In effect, LC domains are feebly connected and are intrinsically soft under shear; thus, the observed rigidity must be strictly assigned to hydrostatic effects. In conclusion, despite the first-order character of the LE/LC transition, the heterogeneous monolayer stresses an unexpected resistance against compression.

Oscillatory Dilational Rheology. To gain further insight into this amazing behavior, we have taken advantage of oscillatory dilational rheology performed on selected monolayer states representing the different monolayer phases. Figure 2 shows a typical time trace for the applied area deformation and the observed stress measured as an excess pressure with respect to an average area unstressed state. The dilational modulus is obtained as the amplitude ratio between stress and strain, while the viscosity is determined from the phase difference between them (see Materials and Methods).

Figure 3 shows viscoelasticity data obtained at variable frequency for DPPC monolayers at room temperature. Similar qualitative behavior was observed at other temperatures (data not shown). This figure summarizes the main results of surface rheology experiments performed upon linear dilation. At the fluid LE state (left panels), no frequency dependence of the dilational elasticity is detected in the probed range. The experimental values are indeed compatible with the quasi-equilibrium values obtained from the compression isotherm (data in Figure 1b). The dilational viscosity (bottom panels) decays in the LE (left) as $\eta \approx \omega^{-1}$, the usual dependence expected for regular fluids at times shorter than a characteristic self-diffusional one, $\tau_{dif} \approx L^2/D$; for a typical lipid at the fluid state, the lateral diffusion coefficient is $D \approx 1$ μm^2/s; thus, for a dilational deformation of size $L = 1$ cm, typically, the monolayer relaxes at times as long as $\tau_{dif} \approx 10^8$ s, well above the time scale probed in oscillatory experiments. At the probed frequencies ($\omega_{exp} \gg \tau_{dif}^{-1}$), lateral diffusion has no time to operate, and upon compression, the monolayer behaves as an elastic body ($\varepsilon(\omega) \approx \varepsilon_0$) with a low viscosity well below the Newtonian limit (at $\omega \ll \tau_{dif}^{-1}$, $\eta \to \varepsilon_0\tau_{dif}$).[51–53] The monolayer is highly fluid as the loss modulus is found in this case to be significantly smaller than the absolute value of dilational elasticity ($\omega\eta \approx 2$ mN/m $\ll \varepsilon_0$).

The central panels in Figure 3 represent the case when domains of the LC phase are present floating on the continuous LE phase (LE/LC coexistence region). Different from the homogeneous LE phase, an elastic behavior characterized by a strong dependence of the dilational modulus on the frequency of the deformation is displayed by these LE/LC heterogeneous monolayers (see Figure 3; top/central panel). At low frequencies, data show a dynamic elasticity modulus compatible with the quasi-equilibrium value measured from the compression isotherm in Figure 1 ($\varepsilon(\omega) \approx \varepsilon_0 \approx 8.5$ mN/m at $\omega \leq 10^{-3}$ s^{-1}). Increasing frequencies lead to a meaningful increase of the compression rigidity, raising a saturation limit at the highest frequency measurable in oscillatory barrier experiments (0.5 s^{-1}, typically). This increase represents a kind of mechanical relaxation, probably due to the presence of structural elements (the domains) able to exchange material with a characteristic time similar to the probed time scale. In previous experimental papers, we have discussed how coexisting domains can induce viscoelastic relaxation[52] and nonlinear response[53] on lipid monolayers. The observed behavior has been rationalized by a simple model of surface diffusion between the domains and the surrounding medium.[61] The only model parameter is a diffusional relaxation time accounting for the characteristic exchange times between domains and the monolayer, τ_{dom}. In the linear limit, the model predicts Maxwell-like relaxation for the elasticity modulus as follows[51,61]

$$\varepsilon(\omega) = \varepsilon_0 + \Delta\varepsilon\frac{\omega^2\tau_{dom}^2}{1 + \omega^2\tau_{dom}^2} \qquad (9)$$

From a fit of the experimental data in Figure 3 (central panel) to eq 9, one obtains a characteristic time, $\tau_{dom} = 140 \pm 20$ s, on the order of that expected for lateral diffusion over a distance given by the domain size (for $L \approx 10$ μm, one gets $\tau_{dif} = L^2/D \approx 100$s). The relaxation strength $\Delta\varepsilon \approx 20$ mN/m is found surprisingly higher than the zero-frequency limit ($\Delta\varepsilon > \varepsilon_0 \approx 8.5$ mN/m), which highlights the importance of the dynamical effect over the quasi-equilibrium energetics. In principle, such a phenomenon might introduce strong dissipative effects, resulting in an effective friction on the order of $\eta_{dom} \approx \Delta\varepsilon\tau_{dom} \approx 10^3$ mN s/m at the LE/LC coexistence region. Although this is on the order of the observed viscosity (central panel; bottom), it remains essentially on the same order as that for the fluid LE phase, where there are no extra effects due to the presence of coexistence domains. Despite of the presence of denser LC domains, the LE/LC biphasic state is indeed much softer than the LC phase, which is characterized by high compression stiffness and much higher viscosity than LE (see right panels in Figure 3).

The fact is that, even if dense LC domains are present, the LE/LC biphasic system preserves the fluidity of the LE phase, ruling out extra dissipative effects arising from either the more viscous LC phase or the diffusive exchanges with it. In other words, we likely observe a macroscopic fluency entirely determined by the high fluidity of the continuous phase. However, concerning rigidity, an obvious question emerges: why does finite rigidity, but smaller than that found for every homogeneous phase, emerge at the LE/LC biphasic state? A plausible response might consider the fact that $\varepsilon(R_{comp})$ increases with the rate of the deformation, $R_{comp} = -\mathrm{d}\ln A/\mathrm{d}t$, between the ideal equilibrium limit ($\varepsilon \to 0$ at $R_{comp} \to 0$) up to the value characteristic for the dominant phase when the monolayer is strained at a rate much faster than the characteristic exchange

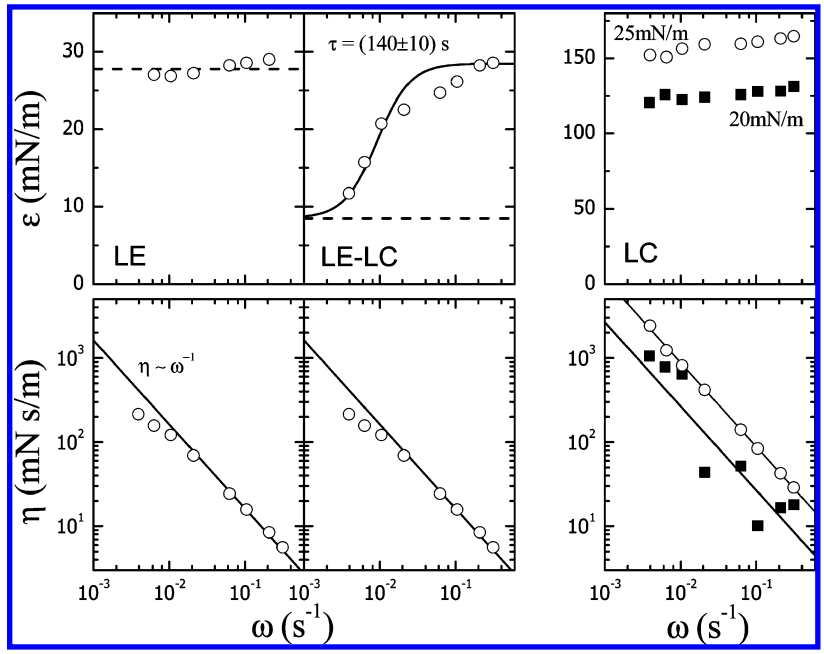

Figure 3. Variation of the dynamical elastic modulus ε (top) and the surface viscosity η (bottom) as a function of the barrier oscillation frequency ω at three different states of the monolayer, LE, LE/LC, and LC, at 25 °C. The discontinuous line represents the equilibrium elastic modulus ε_0 obtained from the $\Pi-A$ isotherm.

rate between the continuous phase and the domains (in the case plotted in Figure 3, $\varepsilon_\infty \rightarrow \varepsilon_{LE}$ at $\omega \gg \tau_{dom}^{-1}$). The compression isotherm corresponds indeed to a kinetic state corresponding to a very slow but finite compression rate ($dA/dt = 10$ cm^2/min; $R_{comp} = 2 \times 10^{-4}$ s^{-1}); therefore, the compression modulus in Figure 1b actually corresponds to a dynamical value including effects from domain resistance to compression. This kinetically controlled behavior goes to the core question addressed here. Ideally, upon compression, the LE phase might freely transform into the LC phase along the phase transition; however, persisting phase coexistence of the monolayer resists compression probably because LC domains do not grow as fast as necessary to incorporate the excess material coming from the compressed LE phase.

Domain Characterization by BAM Microscopy: Nucleation−Growth Mechanism. Getting further insight into the structural basis of such a nontrivial rheological behavior requires BAM microscopy as an adequate visual probe of phase coexistence not requiring fluorescent dopants that could eventually influence phase behavior. Figure 4 shows a sequence of BAM images at different states along the coexistence plateau at 25 °C (see the $\Pi-A$ isotherm in Figure 1).

Although only a few states are displayed in Figure 4, images are continuously recorded as the monolayer is laterally compressed under the action of the Langmuir trough, thus allowing for a continuous monitoring of domain populations at different monolayer states. As the surface pressure is an increasing parameter along the coexistence plateau, we choose it as an easy observable to label a given surface state. As a reference state, the image taken at $\Pi = 8$ mN/m is representative of the homogeneous LE phase. As the plateau region is entered in compressing from its LE boundary ($\Pi_{LE} = 10$ mN/m), the LC phase starts to nucleate as a number of small domains in coexistence with much larger domains, which probably correspond to early nucleated mature domains. A detailed statistical analysis (see Materials and Methods) reveals two-population distributions (see Figure 4; right). A third component appearing at small sizes ($A \leq 5$ μm^2; $R \approx 1$ μm) has been assigned to pixelization noise typical of digital imaging at low light levels.

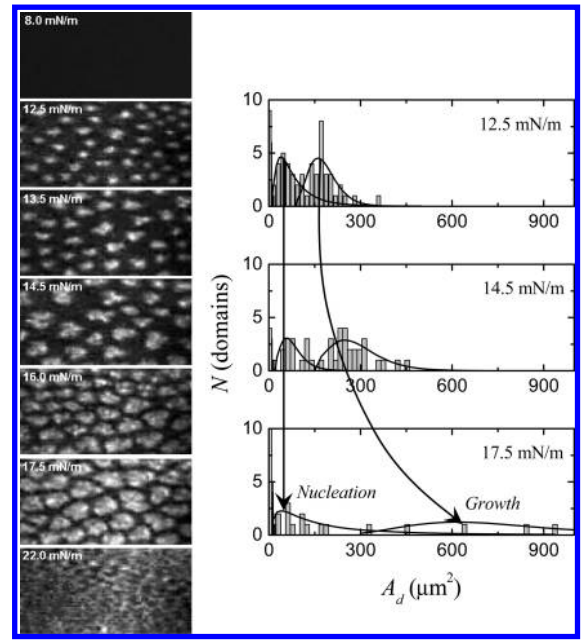

Figure 4. Left: BAM image sequence showing the coexistence of the fluid and gel phases as a function of the surface pressure Π for a DPPC Langmuir monolayer at 25 °C. Right: Histograms showing the number of domains of each size at three different surface pressure states, 12.5, 14.5, and 17.5 mN/m, along the coexistence region. The continuous lines show the coexistence of two populations. The first one is characterized by a constant domain number and area, as expected for a nucleation process; meanwhile, the second one, due to domain growth, shows that N is decreased as A_d is increased.

The main component corresponds to small domains with area $A_{small} \approx 50$ μm^2 (standard deviation = 70%; typical domain radius $R_{small} \approx 4$ μm). Their typical amplitude and size are relatively independent of the compression state, which reveals that small incipient grains are continuously nucleating throughout the biphasic plateau. Near the LE boundary, this small-domain distribution is relatively symmetric with respect to the average size (~50 μm^2) and broadens asymmetrically to larger

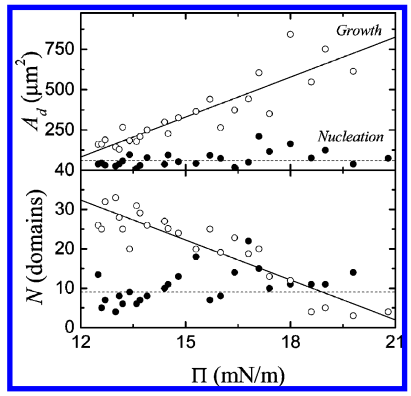

Figure 5. Domain area and number evolution of the two populations as the surface pressure Π is increased for a DPPC Langmuir monolayer at 25 °C. (●) Small domains; (○) mature domains.

areas as the pressure is increased along the coexistence plateau. The second population corresponds to the less numerous but larger domains which progressively ripen to larger and larger size in the course of compression. At the LE boundary, their typical size is $A_{large} \approx 160\ \mu m^2$ ($R_{large} \approx 8\ \mu m$ at $\Pi = 12.5$ mN/m), becoming much larger at the onset of the LC reentrance, $A_{large} \approx 700\ \mu m^2$ ($R_{large} \approx 15\ \mu m$ at $\Pi = 17.5$ mN/m). Figure 5 plots the pressure dependence of the two domain populations, (a) the average size and (b) the absolute amplitude measured as the number of domains with a given size. These data correspond to an average of five different monolayer emplacements, where a near-homogeneous distribution of domains was found. Anyway, data are relatively noisy as domain growth is quite heterogeneous along the monolayer. Indeed, the size and number of domains were recognized early to be nonequilibrium properties.[54] They thus depend on the nucleation process and on the local details and cannot be predicted quantitatively. However, two qualitative features are clearly visible from the data; (1) the LC phase develops through a nucleation/growing mechanism characterized by a continuous nucleation of new grains in parallel with a linear growth of the older ones (their size increases linearly with hydrostatic pressure, $A_{large} \approx \Pi$), and (2) LC phase growth is given by an undetermined combination of domain ripening at the expense of the continuous LE phase and fusion events, the last clearly identified as a decrease of the number of large domains along the biphasic region (see Figure 5b). Although domain aggregation is a minority at the beginning of the coexistence plateau, fusion events become more and more frequent at high coverage. However, even if two or three domains are observed together, they continue to growth independently as quasi-isolated entities. Obviously, domain growth is, in these cases, somehow limited as some domain edges are not exposed to the LE phase, therefore restricting domain growth to peripheral faces. Conversely, domain coalescence events are never observed, as expected for nonfluid domains. This restricts single-domain growth as due to lipid accretion followed by a ripening mechanism.

Despite that individual domains are out-of-equilibrium entities, the macroscopically averaged fraction of the gel phase might follow a quasi-equilibrium behavior characterized by a linear dependence on the molecular area. Figure 6 plots the area dependence of the average gel phase fraction, ϕ_{gel} ($= A_{gel}/A_T$), measured as the ratio of the total area occupied by the LC phase (A_{gel} is calculated as a discrete sum over the population distributions in Figures 4 and 5, which is divided by A_T, the area of the microscopy field). Data in Figure 6 represent averages over five different monolayer emplacements arbitrarily

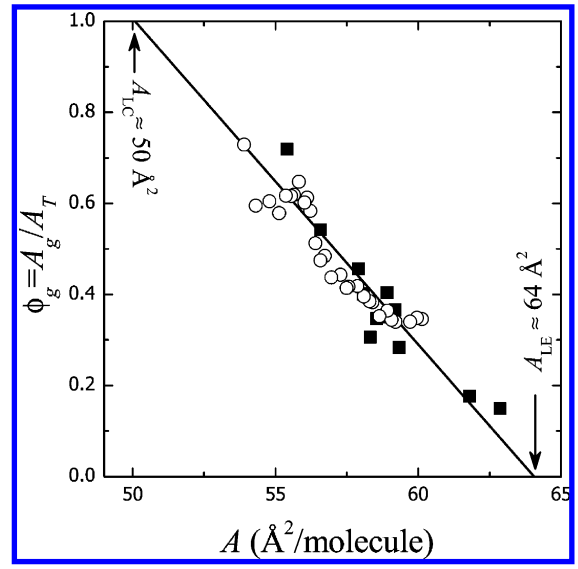

Figure 6. Gel phase fraction evolution with area per molecule for a DPPC Langmuir monolayer at 25 °C. The continuous line shows the linear dependence predicted from the thermodynamic lever rule.

chosen, including data obtained in two independent experiments. These results point out that even if domains are irregularly distributed in the monolayer, the lever rule for the average amount of gel phase is satisfactorily fulfilled. The areas extrapolated to the coexistence boundaries correspond well to the average molecular areas defining the phase coexistence plateau in the compression isotherm (at 25 °C, $A = A_{LE} \approx 64$ Å^2 at $\phi_{gel} \rightarrow 0$ and $A = A_{LC} \approx 50$ Å^2). Such a behavior, observed at the conditions reported here, represents the thermodynamic signature of the macroscopic equilibrium between both phases.[2,4] However, not only the domain distribution and shapes depend sensitively on the nucleation process; also, surface pressure isotherms at the coexistence region have been found to be strongly dependent on the rate of monolayer compression.[37] Indeed, our rheological data point out a domain dynamics profoundly driving the macroscopic mechanical response in the coexistence region. On this idea, we try to identify such a dynamics as a goal to interpret the rate-dependent macroscopic response on a structural basis.

Growth Dynamics. The results above are compatible with a nucleation−growth mechanism. This is the mechanism characteristic for crystalline growth in highly ordered matter with high surface energy at the grain boundaries.[55,56] In the case of lipid monolayers, ordered phases are characterized by a heterogeneous distribution of the line tension giving rise to noncircular domains growing nonsymmetrically along an easy axis. This is the case of DPPC domains which adopt a preferential bean-like shape. However, for fluid domains, line tension effects are hydrostatic and comparatively smaller than those for ordered phases, thus favoring domain coalescence processes which dominate growth dynamics.[3] Our results are compatible with a nucleation−growth scenario which is probably controlled by an activated line tension mechanism limiting accretion over the growing domain. The growth rate might, in this case, follow an Arrhenius dependence as $R_{dom} \approx \tau_{dif}^{-1} \exp(-\sigma L/k_B T)$, where σ is the line tension and L the domain boundary length. For DPPC, one expects $\sigma \approx 0.1$pN, a value typical for LC domains surrounded by the fluid phase.[57] In effect, small domains are qualitatively observed as growing faster than larger ones, which, once grown, seem to raise a quasi-stationary state. Conversely, domain coalescence is a nonactivated process

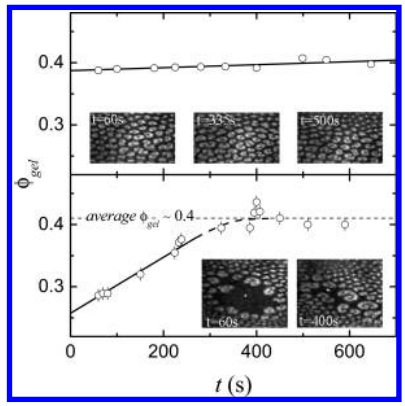

Figure 7. Temporal evolution of the gel phase fraction for a DPPC monolayer at $T = 25$ °C and an average molecular area $A = 55$ Å^2 in the LE/LC coexistence region. The gel phase remains practically constant when there are not defects in the monolayer (top), but it increases when a defect allows domain growth (bottom). Inset: BAM images showing the temporal evolution of the LC domains in the LE phase.

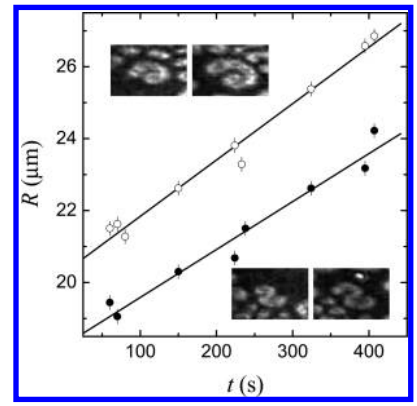

Figure 8. Size evolution with time of two different domains placed in a defect of a DPPC monolayer at $\Pi = 13.5$ mN/m and $T = 25$ °C. Both domains are growing with the same rate, in agreement with the temporal evolution of the gel phase fraction shown in Figure 10.

whose rate is strictly controlled by surface diffusion, that is, $R_{dom} \approx \tau_{dif}^{-1}$.

As initial growth stages are too fast and nucleated grains too small to be resolved, differences are quite difficult to be quantitatively identified in a single domain. However, the existence of defect regions where growth was somehow retarded allows for a qualitative discrimination of the activated process depicted above. Figure 7 shows typical time evolutions of domain sizes in (a) a representative homogeneous region and (b) a pathological region with a long island of the LE phase where small grains have not yet grown. The monolayer is maintained at a constant pressure well inside of the coexistence plateau ($\phi_{gel} \approx 0.4$). Figure 7a shows the case of a typical homogeneous region where domains have already reached a typical mature size; thus, they do not largely evolve during relatively long time lapses. If the time evolution of ϕ_{gel} is recorded, a weak increase is detected with a rate as slow as $R_{growth} = (1/\phi_{gel})(d\phi_{gel}/dt) \approx 10^{-5}$ s^{-1} (see Figure 7a), as expected for a large energy barrier opposed for a domain to become larger and increase its line energy (in these cases, $R \approx 8$ μm, $L = 2\pi R \approx 50$ μm, and thus $\sigma L/k_BT \gg 1$). However, Figure 7b shows a fast growth region where small grains have nucleated recently and a lot of LE phases are yet available. Although both data sets correspond to the same macroscopic state, the last data in Figure 7b could correspond to the infancy of a typical low-density state, raising an equilibrium asymptotic limit, $\phi_{gel} \approx 0.4$, at long time. In this case ($R \approx 4$ μm), the growth rate is $R_{growth} = (1.5 \pm 0.2) \times 10^{-3}$ s^{-1} (see Figure 7b), as expected for small grains growing meaningfully faster than mature domains in homogeneous regions. For the activated mechanism, one expects, $\ln(R_{small}/R_{large}) = 2\pi\sigma(R_{large} - R_{small})/k_BT$. For data in Figure 7, $R_{large} - R_{small} \approx 4$ μm; thus, the ratio $\ln(R_{small}/R_{large}) \approx 10$ is obtained on the same order of magnitude as the difference experimentally observed between data in Figure 7a and b, that is, $\ln(R_{small}/R_{large})_{exp} \approx 7$. Anyway, these qualitative estimations must be only considered as an indirect signature of an energy barrier against domain growth; when domains are small, line tension effects are weaker; therefore, they grow faster as lateral diffusion transports material from the LE phase. As a matter of fact, the diffusive growth rate, $R_{small} \approx \tau_{dif}^{-1} \approx 10^{-3}$ s^{-1} (calculated over a distance $L \approx 30$ μm; $\tau_{dif}^{-1} \approx D/L^2$) is meaningfully slowed down when the domains become larger, $R_{large} \approx 10^{-5}$ s^{-1}. This is clear proof for the existence of a kinetic barrier against further growth. As some large domains are found at the border edge of the defect region in Figure 7b, a detailed analysis of the growth rate of these domains can be performed. Figure 8 plots the time evolution of the sizes of two different domains in this region. This size is measured as the radius of an equivalent circle, that is, $R = (A_{dom}/2\pi)^{1/2}$. At constant lateral pressure, domain sizes are observed to increase linearly with elapsed time. A growth rate can be calculated as $R_{dom} = (1/R)(dR/dt)$, obtaining a value of $R_{dom} = (7.5 \pm 0.7) \times 10^{-4}$ s^{-1}, which is in quantitative agreement with the averaged phase growth rate calculated from Figure 7b; as $A \approx R^2$, one gets $(1/A)(dA/dt) = (2/R)(dR/dt)$; thus $R_{growth} = (1/\phi_{gel})(d\phi_{gel}/dt) = 2R_{dom} \approx 1.5 \times 10^{-3}$ s^{-1}, which is exactly the value of the macroscopically averaged growth rate calculated from Figure 7b. It is worthy noticing that a linear increase of the domain sizes corresponds to an Avrami kinetic equation for the growth of the ordered phase. The Avrami mechanism is dominated by the growth dimensionality, n; at the initial stages, before the stationary mature state is raised (see Figure 7b), the kinetic equation is given by the approximated Göler relationship, $\phi_{gel} \approx kt^n$, with a kinetic constant related to the growth rate of individual domains as $k \approx R_{dom}$.[55,58] For chiral LC two-dimensional domains, as those of DPPC, growth is expected to occur along a preferential direction; thus, $n = 1$, as experimentally observed (see Figures 7 and 8).

Mechanical Behavior of a Raft-Like Domain Distribution: The Plum-Cake Model. The fact that the phase coexistence region was profoundly affected by deformation rates is widely recognized as a prevailing feature in lipid monolayers.[1–4] Most efforts have been devoted to the macroscopic impact of the compression rate on the monolayer structure[1–4] and on the shape and size of the coexistence domains.[37] However, studies issuing the impact of compression rates on domain growth dynamics and their macroscopic mechanical consequences have not been adequately addressed. If the surface phase transition was ideally first-order, the coexistence region might be characterized by a full compressibility ($\varepsilon_0 \equiv 0$). However, when lipid monolayers are laterally compressed at a finite rate, measurable compression rigidity is detected at the coexistence region ($\varepsilon > 0$ at $R_{comp} > 0$). In the case of ordered domains, such as those of the LC phase of DPPC studied here or the lipid rafts hypothesized at real membranes, the membrane might exert finite resistance to compression even at extremely slow deformation rates, contrary to the absolute compliance expected from thermodynamics ($\varepsilon = 0$). We hypothesize noninstantaneous growth dynamics as the key element limiting the capacity of domains to incorporate material from the continuous phase, thus determining the

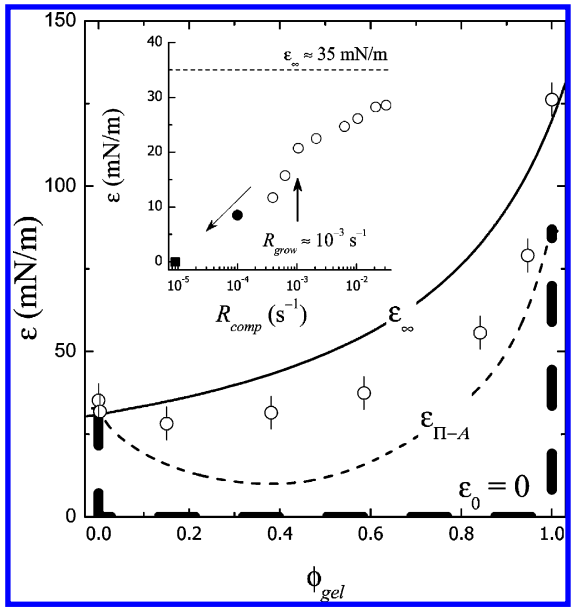

Figure 9. Compression modulus as a function of the gel phase fraction in the coexistence LE/LC region at 25 °C. Dash line shows the values of ε_0 obtained from the $\Pi-A$ isotherm in Figure 1 at a slow but finite compression rate $R_{comp}= 2 \times 10^{-4}$ s^{-1}. Hollow symbols show the dilational modulus ε obtained from surface rheology experiments at a strain rate of $R_{comp}= 2 \times 10^{-2}$ s^{-1}. The continuous line (ε_∞) shows the infinity-rate Plum-cake model prediction, which defines a much stiffer scenario than the one expected for a fully compliant phase-separated monolayer undergoing a first-order LE/LC transition ($\varepsilon_0 = 0$). Inset: Compression modulus as a function of the compression rate. The solid circle corresponds to the apparent equilibrium modulus obtained from our continuous compression isotherm (data from Figure 1b). The solid square at zero compressibility represents the equilibrium value obtained from the quasi-static $\Pi-A$ isotherm of Hifeda and Rayfield (at $R_{comp} = 10^{-5}$ s^{-1}).[15]

resistance of the monolayer to be compressed. Only at extremely slow compression rates, probably off-scale in most practical processes (for the present system, $R_{comp} \ll 10^{-4}$ s^{-1}), lipid domains are able to incorporate material freely, resulting in the thermodynamic limit, $\varepsilon_0 \equiv 0$. In the opposite limit, if strained at high rates, domains have no time for growth, and the monolayer resists against compression, like a rigid material made of hard grains (LC domains) dispersed in a more or less compressible fluid (LE continuous phase). We will immediately recognize this pattern in the mechanical behavior depicted by the DPPC monolayers studied here. Data in Figure 9 consider the finite values of the lateral compression modulus calculated from the $\Pi-A$ isotherm in the coexistence region (ε_0 data plot in Figure 1b). These data actually correspond to a slow but finite compression rate, R_{comp} (= 10 cm^2/min) $\approx 2 \times 10^{-4}$ s^{-1}. We also consider the dilational modulus obtained from surface rheology experiments, $\varepsilon(\omega)$. In the coexistence region, meaningfully higher dynamical elasticities are systematically observed with a dependence on the oscillatory frequency similar to that depicted in Figure 3 (central panel), that is, $\varepsilon(\omega) > \varepsilon_0$. The strain rate involved in these oscillatory experiments is $R_{comp} = \omega u$, u (= dA/A) being the relative deformation (chosen at the linear regime at a 10% strain, $u = 0.1$). For the sake of simplicity, Figure 9 just considers data at a relatively high frequency ($\omega = 0.2$ s^{-1}), corresponding to a strain rate ($R_{comp} = 2 \times 10^{-2}$ s^{-1}) much higher than that involved in continuous compression experiments ($R_{comp} = 2 \times 10^{-4}$ s^{-1}). These high-frequency rheological data (see Figure 3) correspond to the rigid limit mentioned above. At the opposite side, the thermodynamic limit is represented as the ideal first-order transition value (broad dashed lines), with finite values at the phase coexistence boundaries, that is, $\varepsilon_{LE} = 35$ mN/m at $A_{LE} = 64$ Å^2 ($\phi_{gel} = 0$) and $\varepsilon_{LC} = 87$ mN/m at $A_{LC} = 50$ Å^2 ($\phi_{gel} = 1$). The different data in Figure 9 have been plot against the fraction of the gel phase, which is known from the in situ BAM images (see Figure 4).

Figure 9 reveals that the biphasic monolayer behaves stiffer as the external deformations are strained faster. Monolayer dilation along a zero-rate equilibrium path might give rise to a mechanical response characteristic for an ideal compliant system where the gel phase appears with no cost at expense of the LE phase, that is, $\varepsilon_0 \equiv 0$ at $R_{comp} = 0$. However, the real phase transformation involves a complex process in which the gel phase appears rather as incipient grains that later ripen and then grow against a line tension activation barrier. Consequently, a finite time must be elapsed before a mature domain of the LC phase is formed, and more importantly, some energy must be brought in. LC domains have been observed to grow at a rate of $R_{grow} \approx 10^{-3}$ s^{-1}; thus, we observe domains throughout a compression path stressed at a finite rate of $R_{comp} \approx 10^{-4}$ s^{-1}, but nonzero values of the compression modulus are obtained as domains exert some resistance against (values calculated from the derivative of the quasi-plateau $\Pi-A$ path). Even higher values are obtained by compressing faster; particularly, in data from oscillatory rheology experiments (at $u = 0.1$ and $\omega = 0.2$ s^{-1}), the compression rate is $R_{comp} = u\omega = 2 \times 10^{-2}$ s^{-1}, meaningfully higher than the compression modulus obtained at a lower rate. Differently from the full compressibility expected at the coexistence plateau ($\varepsilon_0 = 0$; thick dashes in Figure 9), finite rigidity is found systematically higher at faster compression rates.

This dynamical behavior is exemplified in the inset in Figure 9, which plots data at increasing compression rates. Meaningfully, a nontrivial increase of the elasticity modulus is found with increasing rate, equilibrium being the asymptotic limit at null rate ($\varepsilon \rightarrow 0$ at $R_{comp} \rightarrow 0$). Data at $R_{comp} \gg R_{grow}$ seem to reach a high-rate limit ε_∞, as expected for a relaxation processes due to lipid exchanges between domains and the LE phase occurring at a finite rate.[51,61] Indeed, in the considered case ($\phi_{gel} \approx 0.4$), if one assumes $\varepsilon_\infty \approx 35$ mN/m, a relaxation rate (understood as a characteristic rate for reaching a half relaxation strength) is observed just coinciding with the characteristic rate for domain growth (at $\varepsilon_\infty/2 \approx 17$ mN/m, $R_{rel} \approx R_{grow} \approx 10^{-3}$ s^{-1}). It is worth noticing that this relaxation corresponds to the transport process previously envisaged from rheological data in Figure 3 (performed at a relative compression, $u = 0.1$). In effect, the rheological relaxation time $\tau_{dom} \approx 100$ s exactly corresponds to a characteristic rate $R_{rel} \approx u\omega_{rel} \approx u\tau_{dom}^{-1} \approx 10^{-3}$ s^{-1} $\approx R_{grow}$.

We therefore conjecture on the existence of a domain-driven relaxation process giving rise to the observed dynamic rigidity, which is measured as a stress-stiffening at rates above the characteristic value for domain growth. However, the precise nature of the high-frequency limit deserves further discussion. It might correspond to the maximal stiffness of a heterogeneous system made of rigid grains in a soft continuous matrix. The apparent compressibility of such a composite surface characterized by a surface area A is

$$\varepsilon_\infty^{-1} = -\frac{1}{A}\frac{dA}{d\Pi} \qquad (10)$$

Since we are searching for the instantaneous response, no transport between grains and the fluid phase must be considered;

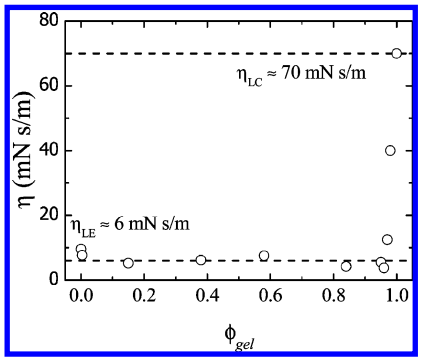

Figure 10. Dilational viscosity as a function of the gel fraction in the LE/LC phase coexistence region.

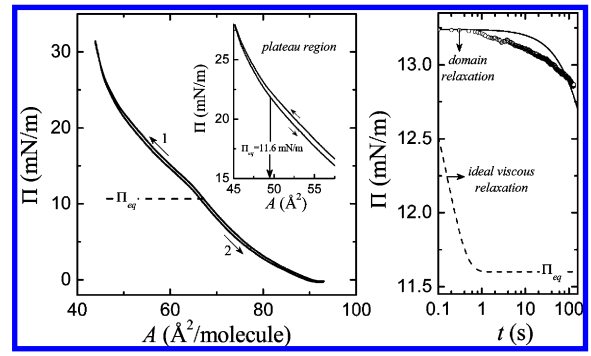

Figure 11. (Left) Typical high-rate compression → expansion (1 → 2) cycle for a DPPC monolayer at 25 °C. Both curves have been obtained at a constant barrier speed of 100 cm²/min ($R = 0.002$ s^{-1}). Inset: Detail of the weak hysteresis detected in the plateau region where coexistence domains are observed. (Right) Constant area relaxation after a sudden compression from the gas state at the plateau region. Symbols correspond to the experimental relaxation data; lines represent predictions for a hypothetical relaxation to the equilibrium plateau pressure ($\Pi_{eq} = 11.6$ mN/m) controlled by (dashed) monolayer viscosity ($\tau_{visc} \approx \varepsilon/\eta \approx 0.17$ s) and (solid) domain growth ($\tau_{dom} \approx 100$ s).

therefore, the whole area is simply given by $A = A_{LC} + A_{LE}$, that is, the area occupied by the hard domains and the expanded phase. Consequently, $dA/A = (dA_{LC} + dA_{LE})/(A_{LC} + A_{LE}) = \phi_{gel}(dA_{LC}/A_{LC}) + (1 - \phi_{gel})(dA_{LE}/A_{LE})$. As each phase is characterized by a different instantaneous compressibility but identical lateral pressure at hydrostatic conditions, eq 10 can be rewritten as follows

$$\varepsilon_{\infty}^{-1} = \frac{1 - \phi_{gel}}{\varepsilon_{\infty}^{(LE)}} + \frac{\phi_{gel}}{\varepsilon_{\infty}^{(LC)}} \qquad (11)$$

Here, the respective compression moduli are defined as $\varepsilon_{\infty}^{(LE)} = -A_{LE}(d\Pi/dA_{LE})$ and $\varepsilon_{\infty}^{(LC)} = -A_{LC}(d\Pi/dA_{LC})$, that is, the instantaneous values corresponding to the homogeneous phases at a given pressure, which might, ideally, correspond to a constant plateaux pressure. However, as coexistence plateaus are not found horizontal at dynamical conditions, a reasonable approximation consists of considering the instantaneous values at the phase coexistence boundaries, that is, $\varepsilon_{\infty}^{(LE)} = \varepsilon_{\infty}(\phi)$ at $\phi_{gel} = 0$ and $\varepsilon_{\infty}^{(LC)} = \varepsilon_{\infty}(\phi)$ at $\phi_{gel} = 1$. Equation 11 represents the compression compliance of a mechanical system with two in-parallel elements, which is the common picture of a composite medium where compressibility is proportionally distributed between hard grains and soft filler, obviously leading to the more abundant and compliant element.[55] This is why we give the name "Plum-cake" to this simple model of composite elasticity, which has been used to estimate the high-rate limit in the coexistence region, using in eq 11 $\varepsilon_{\infty}^{(LE)} = 32$ mN/m and $\varepsilon_{\infty}^{(LC)} = 120$ mN/m, the high-frequency values measured at the phase boundaries in oscillatory experiments (see Figure 9). Predictions from eq 11 have been plot in Figure 9 (ε_{∞}; continuous line), which define an upper limit for the compression rigidity of the biphasic monolayer at strain rates much higher than the characteristic growth rate of the LC domains. Particularly, eq 11 reasonably predicts the high-rate limit depicted in the inset of Figure 9 ($\varepsilon_{\infty} \approx 35$ mN/m at $\phi_{gel} \approx 0.4$).

Viscosity: Fluidity Regulated by the Fluid Matrix. Figure 10 plots the experimental values of the compression viscosity η measured in rheological experiments performed at the coexistence region. Surprisingly, despite the presence of the highly viscous LC phase, throughout the coexistence region, the average viscosity remains low at the value corresponding to the fluid phase, $\eta^{(LE)} \approx 6$ mN s/m. Only at the very proximity of the LC boundary is η observed to suddenly rise up to the high value corresponding to the homogeneous LC phase, $\eta^{(LE)} \approx 70$ mN s/m. This is the flow behavior expected for a fluid continuous phase with floating grains; while grains do not percolate into a quasi-continuous network ($\phi_{gel} \approx 1$), the system is yet able to flow through of the fluid LE phase.

Relaxation Mechanism: Domain Metastability versus Macroscopic Viscosity. As continuous compression states have been found metastable with respect to equilibrium single shot data (see Figure 1), high-rate experiments could provide further dynamical insight into the nature of the relaxation mechanism. In a first attempt, we performed fast compression−expansion cycles displaying markedly nonhorizontal behavior and nonappreciable hysteresis. Figure 11 shows representative data obtained at a relatively high rate ($-dA/dt = 100$ cm²/min; $R_{comp} \approx 0.002$ s^{-1}) between a very dilute state ($\Pi_{ini} = 0$ mN/m) and the onset of the LC re-entrance ($\Pi_{end} = 31$ mN/m). The absence of strong hysteresis upon re-expansion could be interpreted as a dynamical arrest of the metastable states created as a consequence of fast compression. In effect, if as argued above, in-growth domains have no time to follow the hydrostatic pressure field transmitted by the continuous phase, very similar metastable states might exist upon either compression or expansion. Conversely, domains able to partially relax (even equilibrate) upon re-expansion they might give rise to strong hysteresis in the coexistence region. The weak nonreversibility detected in this region, $\Delta\Pi \leq -1$ mN/m (see inset in Figure 11, left), could be simply interpreted as the dissipative consequence of viscous friction at a high rate; in this experiment, the energy dissipated is $E_{dis} \approx \eta R_{comp} \approx 0.1$ mN/m.

Relaxation after a sudden compression at the highest rate accessible to the NIMA instrument ($-dA/dt = 646$ cm²/min; $R_{comp} \approx 0.015$ s^{-1}) provides additional proof of the presence of a domain-related dynamical arrest. In effect, the experimental relaxation curve data in Figure 11 (right panel) are characterized by a long induction period (>1 s) followed by a extremely slow pressure relaxation down to the equilibrium state at times longer than 100s, on the order of the relaxation times measured for domain growth ($\tau_{dom} \approx 100$ s). Alternatively, if a pure viscous relaxation were assumed, neither the energy dissipated by the viscous LC phase ($E_{dis} \approx \eta R_{comp} \leq 0.1$ mN/m) nor the frictional relaxation time ($\tau_{visc} \approx \eta/\varepsilon \approx 0.1$s) are compatible with the observed relaxation, which is found with a higher strength ($E_{rel} \geq 1$ mN/m) and at longer times ($\tau_{rel} \geq 100$s) than a pure viscous mechanism. It is compatible, however, with a domain-induced relaxation mechanism ($\tau_{dom} \approx 100$ s) (see prediction as a solid line in Figure 11, left).

Concluding Remarks

Our experimental design has focused on whether coexistence domains in some way affect monolayer energetics, the combined BAM/rheology results suggesting that the metastability inherent to the nonhorizontal isotherm plateau and the subsequent "apparent" compression rigidity observed at the first-order coexistence region are different consequences of dynamical effects principally arising from the resistance of domains to grow upon fast compression, the LE phase remaining in a metastable compressed state. From the point of view of mechanical relaxation, the material exhibits an amazing behavior characterized by an "elastic" but not viscous relaxation. It is characterized to undergo dynamic stiffening, typical of transport-limited domain relaxation, but conserves the high fluidity typical of the fluid phase. The last is quite rare as limited lipid transport between the continuous phase and the LC domains might cause strong dissipative effects. This apparent paradox arises from thinking of the system as a homogeneous viscoelastic body. However, the "Plum-cake" picture teaches us the composite character of a raft-like distribution of rigid domains in a fluid matrix. Concerning elasticity, the compliant LE phase dominates rigidity as long as it prevails as the predominant phase (see Figure 9; $\varepsilon \approx \varepsilon^{(LE)}$ at $\phi_{gel} < 0.5$); however, the rigid phase also manages some elastic energy. The monolayer becomes mechanically stiff ($\varepsilon \gg \varepsilon^{(LE)}$; $\rightarrow \varepsilon^{(LC)}$) only when the LC phase is predominant with domains close to percolation ($\phi_{gel} \approx 1$). With respect to fluidity, the continuous LE phase, despite the presence of domains rafting inside, is able to connect remote places in the monolayer, thus allowing the monolayer to macroscopically flow through. As a matter of fact, the data in Figure 10 correspond to a composite viscoregulated system at the low fluidity typical of the disordered fluid phase. Although LC domains with a high intrinsic viscosity are present, they are not connected so far; thus, the systems flows through fluid channels made of the continuous fluid phase. The composite system becomes viscous only at the onset of the monophasic re-entrance, where LC domains probably percolate in a continuous network, the LE phase becoming arrested.

From a mechanical point of view, lipid rafts can be conceived to constitute a mechanically compliant environment adequate for accommodating functional protein conformational changes.[29] Although lipid bilayers are usually considered as incompressible sheets, from the present results, we conjecture about the active role of lipid domains on the in-plane compression mechanics. Furthermore, local gradients in lipid distribution within each lipid monolayer are tightly coupled to lateral transport along; thus, the mechanical properties of the membrane might be strongly influenced by the diffusive properties of their lipid components.[59,60] Consequently, our hypothesis is that lipid rafts could be eventually involved in maintaining the structural integrity of the membrane by imposing a diffusive control of lateral lipid exchanges.[61] Although structural stability should require high lipid compaction, we will hypothesize the enhanced compressibility of a "Plum-cake" raft-like distribution competent to endow the mechanical resilience necessary for different cellular processes undergoing large membrane deformations, such as cell division and endocytosis.

Acknowledgment. This work was partially financed by Grants MICINN-FIS2006-01305, CAM-S2005-0505/MAT/0283, MICINN CSD2007-0010 (Consolider Ingenio 2010 en Nanociencia Molecular), MICINN-FIS2006-03525, MICINN-FIS2009-14650-C02-01, and DURSI-SGR2009-1055. L.R.A. thanks CAM for financial support from the FPI program and I. López-Montero for partial financial support from NANOBIO-M (CAM S-0505/MAT/0283) and the Juan de la Cierva program (MICINN). Conclusions from this research have been strongly benefited from fruitful discussions with F. Saguès and R. Reigada on lipid domains and with F. Bresme on monolayer thermodynamics.

References and Notes

(1) Mohwald, H. *Annu. Rev. Phys. Chem.* **1990**, *41*, 441.
(2) Knobler, C. M. *Adv. Chem. Phys.* **1990**, *77*, 397.
(3) McConnel, H. M. *Annu. Rev. Phys. Chem.* **1991**, *42*, 171.
(4) Knobler, C. M.; Desai, R. C. *Annu. Rev. Phys. Chem.* **1992**, *43*, 207.
(5) Dervichian, F. G. *J. Chem. Phys.* **1939**, *7*, 931.
(6) Stallberg-Stenhagen, S.; Stenhagen, E. *Nature* **1945**, *156*, 239.
(7) Florsheimer, M.; Mohwald, H. *Chem. Phys. Lipids* **1989**, *49*, 231.
(8) Phillips, M. C.; Chapman, D. *Biophys. Biochim. Acta* **1968**, *163*, 301.
(9) Albrecht, O.; Gruler, H.; Sackmann, E. *J. Phys. (Paris)* **1978**, *39*, 301.
(10) Cadenhead, D. A., Muller-Landau, F.; Kellner, B. M. J. In *Ordering in Two Dimensions*; Sinha, S. K., Ed.; Elsevier: Amsterdam, The Netherlands, 1980.
(11) Losche, M.; Mohwald, H. *J. Colloid Interface Sci.* **1989**, *131*, 56.
(12) Helm, C. A.; Laxhuber, L.; Losche, M.; Mohwald, H. *Colloid Polym. Sci.* **1986**, *264*, 46.
(13) Pallas, N. R.; Pethica, B. A. *J. Chem. Soc., Faraday Trans. 1* **1987**, *83*, 585.
(14) Pallas, N. R.; Pethica, B. A. *Langmuir* **1985**, *1*, 509.
(15) Hifeda, Y. H.; Rayfield, G. W. *Langmuir* **1992**, *8*, 197.
(16) Georgallas, A.; Pink, D. A. *J. Colloid Interface Sci.* **1982**, *89*, 107.
(17) Roland, C. M.; Zuckermann, M. J.; Georgallas, A. *J. Chem. Phys.* **1987**, *86*, 5852.
(18) Jain, M. K.; White, H. B. *Adv. Lipid Res.* **1977**, *15*, 60.
(19) Klausner, R. D.; Kleinfeld, A. M.; Hoover, R. L.; Karnovsky, M. J. *J. Biol. Chem.* **1980**, *255*, 1286.
(20) Dotti, C. G.; Parton, R. G.; Simons, K. *Nature* **1991**, *349*, 158.
(21) Edidin, M. *Annu. Rev. Biophys. Biomol. Struct.* **2003**, *32*, 257.
(22) Simons, K.; Vaz, W. L. C. *Annu. Rev. Biophys. Biomol. Struct.* **2004**, *33*, 269.
(23) Van Meer, G. *EMBO J.* **2005**, *24*, 3159.
(24) Damel, R. A.; van Kessel, G.; Zwaal, W. S.; Roelofsen, R. F.; Van Beenen, B. *Biochim. Biophys. Acta* **1975**, *406*, 97.
(25) Elgsaeter, A.; Mikkelsen, A. *AIP Conf. Proc.* **1991**, *226*, 349.
(26) Rachana, R.; Banerjee, R. *Colloids Surf., B* **2006**, *50*, 9.
(27) Gericke, A.; Flach, C. R.; Mendelsohn, R. *Biophys. J.* **1997**, *73*, 492.
(28) Disher, B. M.; Schief, W. R.; Vogel, V.; Hall, S. B. *Biophys. J.* **1999**, *77*, 2051.
(29) Yan, W.; Piknova, B.; Hall, S. B. *Biophys. J.* **2005**, *89*, 306.
(30) Gerber, F.; Krafft, M. P.; Vandamme, T. E.; Goldmann, M.; Fontaine, P. *Biophys. J.* **2006**, *90*, 3184.
(31) Rasband, W. S. ImageJ; U.S. NIH: Bethesda, MD, http://rsb.info.nih.gov/ij/ (1997−2009).
(32) Sundaram, S.; Ferri, J. K.; Vollhardt, D.; Stebe, K. J. *Langmuir* **1998**, *14*, 1208.
(33) Zhao, J.; Vollhardt, D.; Brezesinski, G.; Siegel, S.; Wu, J.; Li, J. B.; Miller, R. *Colloids Surf., A* **2000**, *171*, 175.
(34) Ignés-Mullol, J.; Claret, J.; Sagués, F. *J. Phys. Chem. B* **2004**, *108*, 612.
(35) Monroy, F.; Rivillon, S.; Ortega, F.; Rubio, R. G. *J. Chem. Phys.* **2001**, *115*, 530.
(36) Hilles, H.; Monroy, F.; Bonales, L. J.; Ortega, F.; Rubio, R. G. *Adv. Colloid Interface Sci.* **2006**, *122*, 67.
(37) Klopfer, K. J.; Vanderlick, T. K. *J. Colloid Interface Sci.* **1996**, *182*, 220.
(38) Baldyga, D. D.; Dluhy, R. A. *Chem. Phys. Lipids* **1998**, *98*, 81.
(39) Nagle, J. F. *Faraday Discuss. Chem. Soc.* **1986**, *81*, 151.
(40) Kaganer, V. M.; Möhwald, H.; Dutta, P. *Rev. Mod. Phys.* **1999**, *71*, 779.
(41) Keller, D. J.; Korb, J. P.; McConnell, H. M. *J. Phys. Chem.* **1987**, *91*, 6417.
(42) McConnell, H. M.; Moy, V. T. *J. Phys. Chem.* **1988**, *92*, 4520.
(43) Andelman, D.; Brochard, F.; Joanny, J. F. *J. Chem. Phys.* **1987**, *86*, 3672.
(44) Mayer, M. A.; Vanderlick, T. K. *Langmuir* **1992**, *8*, 3131.
(45) This compression rate can be considered typically slow in $\Pi-A$ experiments; more than 1 h is required to record a full isotherm at this rate.

(46) Miller, R., Liggieri, L., Eds. *Interfacial Rheology*; Brill: The Netherlands, 2009.

(47) López-Montero, I.; Vélez, M.; Monroy, F.; Devaux, P. *Biochim. Biophys. Acta* **2009** Accepted.

(48) Abraham, B. M.; Ketterson, J. K. *Langmuir* **1985**, *1*, 708.

(49) Behroozi, F. *Langmuir* **1996**, *12*, 2289.

(50) Miller, A.; Mohwald, H. *J. Chem. Phys.* **1987**, *86*, 4528.

(51) Monroy, F.; Kahn, J. G.; Langevin, D. *Colloids Surf.* **1998**, *143*, 251.

(52) López-Montero, I.; Arriaga, L. R.; Monroy, F.; Rivas, G.; Tarazona, P.; Vélez, M. *Langmuir* **2008**, *24*, 4065.

(53) López-Montero, I.; Arriaga, L. R.; Rivas, G.; Vélez, M.; Monroy, F. *Chem. Phys. Lipids* **2010**, *163*, 56.

(54) Kirstein, S.; Möhwald, H.; Shimomura, M. *Chem. Phys. Lett.* **1989**, *154*, 303.

(55) Christian, J. W. *Theory of Transformations in Metals and Alloys*; Pergamon: Oxford, U.K., 1981.

(56) Offerman, S. E.; van Dijk, N. H.; Sietsma, J.; Grigull, S.; Lauridsen, E. M.; Margulies, L.; Poulsen, H. F.; Rekveldt, M. Th.; van der Zwaag, S. *Science* **2002**, *298*, 1003.

(57) Marrink, S. J.; Risselada, J.; Mark, A. E. *Chem. Phys. Lipids* **2005**, *135*, 223.

(58) Gedde, U. W., Ed. *Polymer Physics*; Capman and Hall: London, 1995.

(59) Jones, M. N.; Chapman, D., Eds. *Micelles, Monolayers and Biomembranes*; Wiley-Liss: New York, 1995.

(60) Gaines, G. L., Ed. *Insoluble Monolayers at Liquid-Gas Interfaces*; Wiley-Interscience: New York, 1966.

(61) Arriaga, L. R.; López-Montero, I.; Rodríguez-García, R.; Monroy, F. *Phys. Rev. E* **2008**, *77*, 061918.

JP9118953